

Generation of arbitrary vector Bessel beams on higher-order Poincaré spheres with an all-dielectric metasurface

Jiaqi Yang ^{*}, Tommi K. Hakala, and Ari T. Friberg

Institute of Photonics, University of Eastern Finland, P.O. Box 111, FI-80101 Joensuu, Finland



(Received 20 May 2022; accepted 9 August 2022; published 22 August 2022)

Vector Bessel beams may have a spatially varying polarization state combined with a Bessel-type transversal intensity profile. Such beams can carry both spin angular momentum and orbital angular momentum (OAM) and be characterized by points on higher-order Poincaré (HOP) spheres. We report a method to produce vector Bessel beams on any point of a HOP sphere of any topological charge by utilizing only a single all-dielectric planar metasurface. Specifically, by a proper choice of the input polarization and distance from the metasurface, the entire HOP sphere surface can be covered. The proposed method is simple and efficient and applies to any n th-order HOP sphere. Furthermore, it yields an extremely high OAM mode purity. Our paper demonstrates a robust approach for generating arbitrary high-quality vector Bessel beams and will likely inspire future applications ranging from optical manipulation to laser beam engineering.

DOI: [10.1103/PhysRevA.106.023520](https://doi.org/10.1103/PhysRevA.106.023520)

I. INTRODUCTION

Following the discovery of Bessel beams in 1987 [1], propagation invariant optical fields of many different types—scalar, electromagnetic, partially coherent, nonstationary (pulsed)—have been extensively studied [2]. Such beam fields have found numerous uses in manufacturing [3] and various areas of optics [4–8], owing to their finite beam width, non-diffractive propagation, high intensity extended focus over considerable distances, and general regenerative properties behind obstacles. Vector Bessel beams may also possess transversally varying polarization states [9,10]. Typically, vector Bessel beams are characterized by two common forms of polarization states, namely, the radial and azimuthal polarizations. Polarization transformation between these states in vector Bessel beams normally requires a complex combination of wave plates [11]. Besides, Bessel-beam generation itself also necessitates conventional lens pairs, diffractive optical elements, or spatial light modulators [12–15], which are bulky and unavoidably affect beam quality and often reduce energy efficiency.

The polarization states of vector Bessel beams are conveniently described by points on a higher-order Poincaré (HOP) sphere [16]. In contrast to the classical Poincaré sphere, the n th-order HOP sphere is a generalized Bloch sphere with two orthogonal circular polarization states represented at the poles. The HOP sphere poles correspond to vortex beams of uniform polarization distribution, a phase pattern of the form $e^{in\varphi}$ (φ is the azimuthal angle), and a nonuniform intensity profile. The other points on HOP spheres correspond to different elliptical and linear polarizations. Importantly, beams characterized by the HOP sphere can carry both spin angular

momentum (SAM) and orbital angular momentum (OAM), respectively [16,17]. There are many approaches to generate HOP sphere beams, including the use of q plates and wave plates in a laser cavity [18], optical fibers [19], liquid crystals [20], and other methods [21–23].

Metasurfaces, which consist of subwavelength scale resonator arrays, are typically flat and smaller in size than conventional optical elements. Therefore, metasurfaces offer an appealing miniaturized approach for generating various scalar or vectorial beams. For instance, rectangular nanopillars have been utilized to produce hybrid-order Poincaré beams (but not higher-order Poincaré Bessel beams) [24]. Demonstrations cover both microwave and optical regimes [25–33]. However, these setups only realize beams which correspond to certain specific points on a HOP sphere. Thus, although numerous designs have been investigated, a general approach is put forward here to efficiently create any vector Bessel beam on an arbitrary HOP sphere by means of a single metasurface.

In this paper, we demonstrate theoretically a construction of an all-dielectric metasurface for arbitrary vector Bessel-beam generation. By controlling a wave-plate rotation angle for incident polarization state selection and choosing an appropriate distance behind the metasurface, we can create Bessel beams that cover the entire surface of a HOP sphere. Moreover, the simulations indicate that the metasurface design strategy is suitable for arbitrary n th-order HOP spheres, whereas maintaining a high beam quality. For example, in the case of $n = +2$, we find mode purity in excess of 99.8% for circularly polarized vortex Bessel beams carrying OAM in analogy with the Laguerre-Gaussian modes [17]. Our paper provides a generic approach for metasurface-based polarization control and may have great potential in various applications, such as optical trapping and spanning, laser manufacturing, and communication.

^{*}jiaqi.yang@uef.fi

II. PRINCIPLE OF GENERATING VECTOR BESSEL BEAMS ON HOP SPHERES

In cylindrical coordinates (r, φ, z) the scalar form of a Bessel beam can be written as [2]

$$E(r, \varphi, z) = E_0 e^{ik_z z} e^{in\varphi} J_n(k_r r), \quad (1)$$

where E_0 is a complex amplitude, k_z and k_r are the axial and radial wave vectors, related to the vacuum wave number as $k_0 = \sqrt{k_z^2 + k_r^2}$, and $J_n(\cdot)$ is the Bessel function of the first kind and order n . The integer n is the spiral phase order (topological charge) with respect to the main axis z of propagation. The factor $e^{in\varphi}$, thus, indicates that the Bessel beam of Eq. (1) is capable of carrying orbital angular momentum and represents an optical vortex. All higher-order Bessel beams ($n \neq 0$) have a phase singularity and lead to zero-field intensity along the propagation axis. Scalar Bessel beams can be created by refracting an incident plane wave conically at equal angles by an axicon [34,35] (the so-called axicon line image [36]), whereas a phase profile may be added through a phase plate. The whole approach may also be realized by means of a single computer hologram [37] or a programmable spatial light modulator (SLM).

A radially polarized vector Bessel beam can be decomposed in the basis of right (RCP) and left (LCP) circularly polarized Bessel beams,

$$|R\rangle = \frac{1}{\sqrt{2}} \begin{bmatrix} 1 \\ -i \end{bmatrix}, \quad |L\rangle = \frac{1}{\sqrt{2}} \begin{bmatrix} 1 \\ i \end{bmatrix}, \quad (2)$$

with opposite spiral phase profiles $(\pm\varphi)$ [10]. Such a light field can be written as

$$\begin{aligned} \mathbf{E}(r, \varphi, z) &= \frac{1}{\sqrt{2}} E_0 e^{ik_z z} J_1(k_r r) \{e^{i\varphi} |R\rangle + e^{-i\varphi} |L\rangle\} \\ &= E_0 e^{ik_z z} J_1(k_r r) \begin{bmatrix} \cos \varphi \\ \sin \varphi \end{bmatrix}. \end{aligned} \quad (3)$$

Since the RCP and LCP states may be viewed as the decomposed components of horizontally or x -polarized light $(|R\rangle + |L\rangle)/\sqrt{2}$, changing the incident linear polarization direction will result in a different polarization distribution for the emerging light (see Sec. III). For instance, y -polarized light $i(|R\rangle - |L\rangle)/\sqrt{2}$ leads to an azimuthally polarized vector Bessel beam. With spiral phase profiles $\pm n\varphi$ (n is an integer), we find a superposition for the n th-order radially polarized vector Bessel beam as

$$\begin{aligned} \mathbf{E}(r, \varphi, z) &= \frac{1}{\sqrt{2}} E_0 e^{ik_z z} J_n(k_r r) \{e^{in\varphi} |R\rangle + e^{-in\varphi} |L\rangle\} \\ &= E_0 e^{ik_z z} J_n(k_r r) \begin{bmatrix} \cos(n\varphi) \\ \sin(n\varphi) \end{bmatrix}. \end{aligned} \quad (4)$$

Fields of this kind can be generated by employing SLMs or metasurfaces [14,25] which combine an axicon and spiral phase plates of opposite orders.

On introducing different axial phases for the RCP and LCP components, whereas retaining the Bessel-like nature, Eq. (4)

is modified into the form

$$\begin{aligned} \mathbf{E}(r, \varphi, z) &= \frac{1}{\sqrt{2}} E_0 e^{ik_z z} J_n(k_r r) \\ &\quad \times \{e^{i\Delta} e^{in\varphi} |R\rangle + e^{-i\Delta} e^{-in\varphi} |L\rangle\} \\ &= E_0 e^{ik_z z} J_n(k_r r) \begin{bmatrix} \cos(n\varphi + \Delta) \\ \sin(n\varphi + \Delta) \end{bmatrix}, \end{aligned} \quad (5)$$

with 2Δ representing the phase difference between the two Bessel beams. Provided Δ is arranged to depend on the axial propagation distance, i.e., $\Delta = \Delta(z)$, then instead of varying the incident light's polarization direction, the phase difference $\Delta(z)$ leads to polarization state changes of the output vector Bessel beam upon propagation. When $n = 1$ and the phase difference $\Delta(z)$ varies from 0 to $\pi/2$, the polarization state of the Bessel beam changes from radial to azimuthal. Conceptually, whereas $\Delta(z)$ ranges between 0 and π , the output Bessel beam's polarization state will cover the entire HOP sphere equator as shown in Fig. 1(a).

Importantly, realizing generalized vector Bessel-beam modes on arbitrary HOP spheres requires control over two degrees of freedom, which in spherical coordinates are the azimuthal and the polar angle. Our solution allows us to adjust the phase difference (2Δ) between two opposite circular polarizations necessary for controlling the azimuthal angle, whereas variation of the input polarization state enables us to control the polar angle (2α) as is illustrated in Fig. 1(a). The concept for generating arbitrary vector Bessel beams on HOP spheres is shown in Fig. 1(b). A QWP of rotation angle β modifies the initial horizontal polarization into the required polarization state (if $\beta = \pm 45^\circ$, the output states are LCP and RCP). On traversing the QWP the beam illuminates the metasurface, which is designed to add different axicon phases to the RCP and LCP components of an incident Gaussian beam and, thus, will convert both into Bessel-type beams whereas maintaining the 2Δ phase difference.

By properly controlling the rotation angle β and choosing the propagation distance z , this method allows us to cover the entire HOP sphere. Under these circumstances, the output beam field can finally be represented as

$$\begin{aligned} \mathbf{E}(r, \varphi, z) &= \frac{1}{\sqrt{2}} E_0 e^{ik_z z} J_n(k_r r) \\ &\quad \times \{\cos \alpha e^{i\Delta} e^{in\varphi} |R\rangle + \sin \alpha e^{-i\Delta} e^{-in\varphi} |L\rangle\}. \end{aligned} \quad (6)$$

The relationship between the polar angle α and the QWP rotation angle β is $\alpha = \pi/4 + \beta$. The emergent beam may, consequently, be represented as

$$|\Psi_{\text{out}}\rangle = \cos \alpha e^{i\Delta} |R_n\rangle + \sin \alpha e^{-i\Delta} |L_n\rangle, \quad (7)$$

where $|R_n\rangle = e^{in\varphi} |R\rangle$ and $|L_n\rangle = e^{-in\varphi} |L\rangle$ are the RCP and LCP vector Bessel beams corresponding to the north and south poles, respectively, on the HOP sphere of topological charge n .

The connection between axial phase difference 2Δ and the propagation distance z can be understood from the properties of axicons [35]. The geometric length Z_{max} of the axicon line focus is given by [37]

$$Z_{\text{max}} = \frac{R_{\text{max}} d}{\lambda}, \quad (8)$$

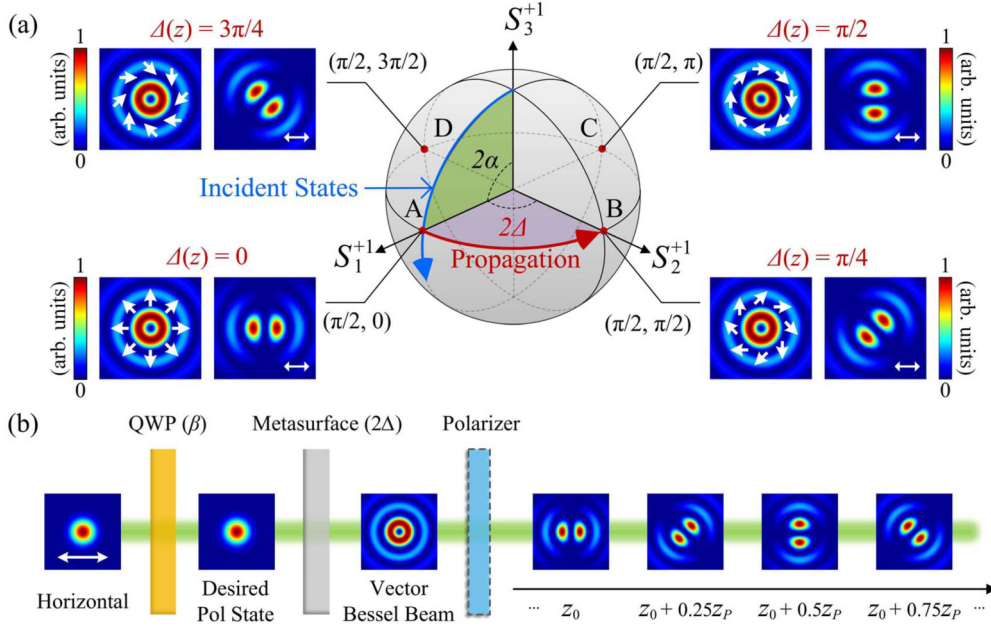


FIG. 1. (a) Polarization vector states and beam intensities at special positions on the equator of the $n = 1$ HOP sphere. Examples of the lobe patterns are shown for transmitted intensity passing through a linear polarizer oriented horizontally (white arrow). The positions are labeled by their $(2\alpha, 2\Delta)$ parameter values. (b) Conceptual illustration of an arbitrary vector Bessel-beam mode generation on a HOP sphere. The desired polarization state is achieved by transmitting a horizontally polarized Gaussian beam through a quarter wave plate (QWP) rotated at angle β . A metasurface then converts the incident beam into a Bessel type, whereas simultaneously introducing a 2Δ phase difference between the RCP and the LCP components. This results in varied vector states along propagation. This two-step process can cover the entire arbitrary HOP sphere.

where R_{\max} is the radius of the metasurface, d is the radial period of the axicon, and λ is the operating wavelength. In our case, we apply two axicons of different radial periods, so Z_{\max} is restricted by the smaller d . For specificity, we take $d_1 < d_2$ with d_1 and d_2 being associated with the RCP and LCP beams, respectively. The length Z_{\max} from Eq. (6) thereby attains the value of $R_{\max}d_1/\lambda$. With the different radial periods d_1 and d_2 , the phase distributions for the axicons read as

$$\phi_1(r) = \frac{2\pi r}{d_1}, \quad \phi_2(r) = \frac{2\pi r}{d_2}, \quad (9)$$

and the phase difference $\Delta\phi(r)$ at a specific radius r is

$$2\Delta\phi(r) = \phi_1(r) - \phi_2(r) = \frac{2\pi r(d_2 - d_1)}{d_1 d_2}. \quad (10)$$

The axicon phase $\phi_1(r)$ is the sum of $\phi_2(r)$ and $2\Delta\phi(r)$. So, the effect of $\phi_1(r)$ can be viewed as refracting incident planar light into an angle θ , whereas contributing a radially dependent phase difference $\Delta\phi(r)$. The refraction angle θ refers to $\lambda = d_2 \sin \theta \approx d_2 r/z$ [11] as is illustrated in Fig. 2. Using the relation $r = z\lambda/d_2$, the quantity $\Delta\phi(r)$ can be converted into the z -dependent phase $\Delta(z)$ as

$$\Delta(z) = \frac{\pi z \lambda (d_2 - d_1)}{d_1 d_2^2}. \quad (11)$$

The phase difference $\Delta(z)$ between the RCP and the LCP beams along the propagation axis leads to the alternating polarization state. The distance z_P between two identical polarization states requires that $\Delta(z_2) - \Delta(z_1) = \pi$

whereby z_P is given by

$$z_P = \frac{d_1 d_2^2}{\lambda (d_2 - d_1)}. \quad (12)$$

Obviously, z_P must be smaller than Z_{\max} , and the beam mode evolution on a HOP sphere can be only found in the overlapping Bessel-beam region.

III. METASURFACE DESIGN

For vector Bessel-beam generation on HOP spheres, we first consider an incident linearly polarized beam propagating along the z axis. The beam can be decomposed into the circular basis of $|L\rangle$ and $|R\rangle$ [24]. In our case, we require the

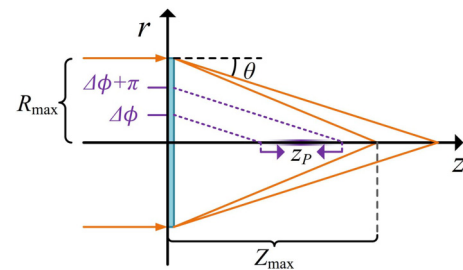


FIG. 2. Incident light is refracted by the two axicons into approximately the same angle θ . The phase-shift $\Delta\phi(r)$ leads to changes in the polarization state along the z axis. The distance z_P , corresponding to a π variation in $\Delta\phi(r)$, is the axial polarization modulation period.

metasurface to perform the transformation,

$$\mathbf{T}|L\rangle = e^{i\phi_1(r)}|R_n\rangle, \quad \mathbf{T}|R\rangle = e^{i\phi_2(r)}|L_n\rangle, \quad (13)$$

where $|R_n\rangle = e^{in\varphi}|R\rangle$ and $|L_n\rangle = e^{-in\varphi}|L\rangle$ as before, and $n\varphi$ is an azimuthal phase. The quantities $\phi_1(r)$ and $\phi_2(r)$ are the phase profiles of two axicons. The circularly polarized input basis, thus, transforms into Bessel-type beams with axial phase difference and azimuthal phase factors $e^{\pm in\varphi}$, where n is an integer. The two output circularly polarized (LCP and RCP) Bessel beams have helical phase fronts of order n , but opposite handedness and annular intensity profiles with a phase singularity ($n \neq 0$).

By making direct use of Eqs. (13), we can readily find the Jones matrix \mathbf{T} characterizing the metasurface [33]. The result is

$$\mathbf{T} = \frac{1}{2} \begin{bmatrix} e^{i(n\varphi+\phi_1)} + e^{i(-n\varphi+\phi_2)} & -ie^{i(n\varphi+\phi_1)} + ie^{i(-n\varphi+\phi_2)} \\ -ie^{i(n\varphi+\phi_1)} + ie^{i(-n\varphi+\phi_2)} & -e^{i(n\varphi+\phi_1)} - e^{i(-n\varphi+\phi_2)} \end{bmatrix}, \quad (14)$$

where we have suppressed, for brevity, the radial variable r of the axicon profiles ϕ_1 and ϕ_2 . The matrix \mathbf{T} provides the mapping from a linearly polarized input to a desired vector Bessel beam. It follows at once from Eq. (14) that \mathbf{T} is unitary and, therefore, admits a representation as $\mathbf{T} = \mathbf{V}\mathbf{D}\mathbf{V}^\dagger$, where \mathbf{D} is a diagonal matrix containing the eigenvalues of \mathbf{T} and \mathbf{V} is a unitary matrix consisting of the associated eigenvectors [33]. If we write $a = n\varphi + \phi_1$ and $b = -n\varphi + \phi_2$, we find that

$$\mathbf{D} = \begin{bmatrix} e^{i(a+b)/2} & 0 \\ 0 & e^{i[(a+b)/2-\pi]} \end{bmatrix}, \quad (15)$$

$$\mathbf{V} = \begin{bmatrix} \cos[(a-b)/2] & -\sin[(a-b)/2] \\ \sin[(a-b)/2] & \cos[(a-b)/2] \end{bmatrix}. \quad (16)$$

Physically, the diagonal matrix \mathbf{D} represents phase delays δ_x and δ_y in the x and y coordinates, whereas the matrix $\mathbf{V} = \mathbf{R}(-\theta)$ can be considered as a counterclockwise rotation by angle θ on the xy plane whereby $\mathbf{V}^\dagger = \mathbf{R}(\theta)$. Hence, the metasurface transmission matrix \mathbf{T} assumes the factored form

$$\mathbf{T} = \begin{bmatrix} \cos \theta & -\sin \theta \\ \sin \theta & \cos \theta \end{bmatrix} \begin{bmatrix} e^{i\delta_x} & 0 \\ 0 & e^{i\delta_y} \end{bmatrix} \begin{bmatrix} \cos \theta & \sin \theta \\ -\sin \theta & \cos \theta \end{bmatrix}, \quad (17)$$

where

$$\delta_x = \frac{1}{2}(\phi_1 + \phi_2), \quad (18)$$

$$\delta_y = \frac{1}{2}(\phi_1 + \phi_2) - \pi, \quad (19)$$

$$\theta = n\varphi + \frac{1}{2}(\phi_1 - \phi_2). \quad (20)$$

In the Cartesian reference frame, the polar angle φ in the spiral phase and the axicon phase profiles ϕ_1 and ϕ_2 in Eqs. (18)–(20) are

$$\varphi = \arctan\left(\frac{y}{x}\right), \quad (21)$$

$$\phi_1 = \sqrt{x^2 + y^2} \left(\frac{2\pi}{d_1}\right), \quad (22)$$

$$\phi_2 = \sqrt{x^2 + y^2} \left(\frac{2\pi}{d_2}\right). \quad (23)$$

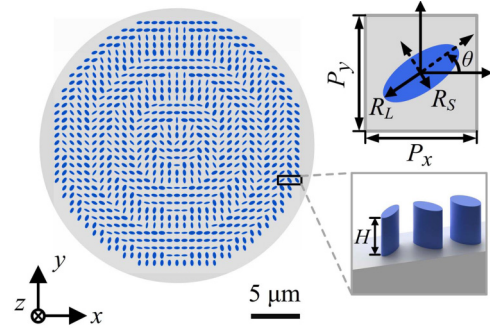


FIG. 3. Schematic representation of the metasurface platform for arbitrary vector Bessel-beam beam generation. The metasurface is composed of elliptical nanopillars of equal height $H = 800$ nm, but different radii R_L , R_S , and rotation angles θ . The lattice constants in x and y directions are equal $P_x = P_y = 650$ nm. The operating wavelength $\lambda = 1550$ nm is in the telecom range.

For the two axicons, the radial phase profiles $\phi_1(x, y)$ and $\phi_2(x, y)$ and their corresponding radial gradients $2\pi/d_1$ and $2\pi/d_2$ are different. With a single axicon (ϕ_1) we obtain a (radially polarized) vector Bessel beam as in Eq. (3), but combining the effects of the two axicons (ϕ_1 and ϕ_2) we are able to generate a spatially varying polarized vector Bessel beam as given by Eq. (5) and characterized in Eq. (12). Such complex polarization-related beam profiles can be realized with metasurfaces, which consist of periodic subwavelength nanostructures and are capable of providing controllably the required inhomogeneous spatial phase distributions.

A schematic of the metasurface platform for vector Bessel-beam creation is shown in Fig. 3. The metasurface is composed of a layer of silicon nanopillars, arranged in a two-dimensional subwavelength array. Each unit of lattice constant $P = P_x = P_y$ houses a single nanopillar with an elliptical cross section. All nanopillars have the same height H but may be freely designed in different sizes and orientations to the control rotation angle θ and the two orthogonal phase delays δ_x and δ_y . The elliptical nanopillars, enabling phase coverage from 0 to 2π , operate, such as waveguides with different effective refractive indices along the two ellipse radii. Due to silicon's high refractive index ($n = 3.478$ at $\lambda = 1550$ nm [38]), the incident light is mainly confined into the nanopillars and further affected by a radius-dependent phase delay [39]. In addition, when the ellipse radii satisfy $2R \approx \lambda/n$ (λ is the free-space wavelength), a strong magnetic dipole resonance will effectively be excited and accompany a π -phase change [40]. We find that all desired δ_x and δ_y values can be obtained by properly choosing the geometrical parameters of the nanopillars.

To evaluate nanopillar phase modulation capacity, we employ finite difference time-domain numerical simulation (Lumerical). We first explore different radii R_L and R_S of a single nanopillar and record the phase shift. For δ_x we consider x -polarized and for δ_y y -polarized plane-wave incidence [see Fig. 4(a)]. The radii studied range between 50 and 300 nm, and their corresponding phase delay combination δ_x , δ_y forms a library to enable our size parameter selection [as shown in Figs. 4(b) and 4(c)]. The field transmittance as a function of R_L and R_S is plotted in Figs. 4(d) and 4(e). For most radius

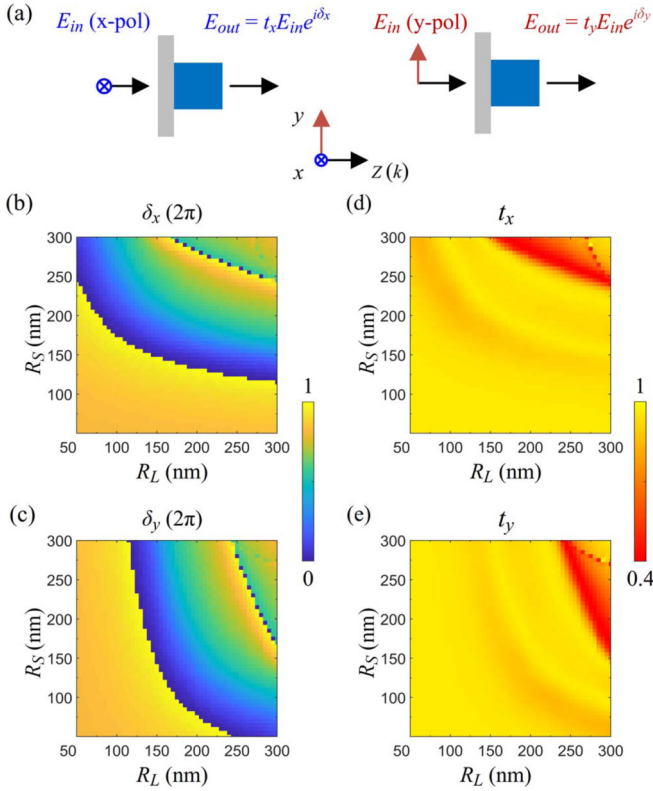


FIG. 4. (a) Schematic of elliptical nanopillar field modulation. Light in x and y polarizations experiences different changes in transmitting the nanopillar. (b) and (c) Simulated phase delays and (d) and (e) transmittances of a single nanopillar of varying radii R_L and R_S [(b) and (d): x -polarized incidence, (c) and (e): y -polarized incidence].

pairs, both transmittances t_x and t_y exhibit large values, which is crucial for high-energy efficiency. In Table I, 13 nanopillars that cover a 2π -phase range are chosen from the data library, and their radii as well as transmittances $T = (t_x + t_y)/2$ are listed. The simulated phase delays δ_x and δ_y for these selected nanopillars are depicted in Fig. 5(a), confirming the full 2π coverage. Meanwhile, a constant π -phase difference between δ_x and δ_y is obtained as required by Eqs. (18) and (19). In Fig. 5(b), by rotating each selected nanopillar with θ , a phase $\varphi = 2\theta$ (so-called Pancharatnam-Berry phase) is added to the wavefront [41]. To summarize, each unit of the metasurface has three degrees of freedom (size, ellipticity, and orientation of the nanopillar) that allow a complete phase control for realizing the \mathbf{T} matrix discussed above. We note

TABLE I. Nanopillar radii (nm) and transmittances.

Number	R_L	R_S	T	Number	R_L	R_S	T
1 and 13	260	90	0.94	7	90	260	0.94
2	270	100	0.97	8	100	270	0.97
3	260	120	0.98	9	120	260	0.98
4	270	130	0.98	10	130	270	0.98
5	270	140	0.97	11	140	270	0.97
6	280	150	0.98	12	150	280	0.98

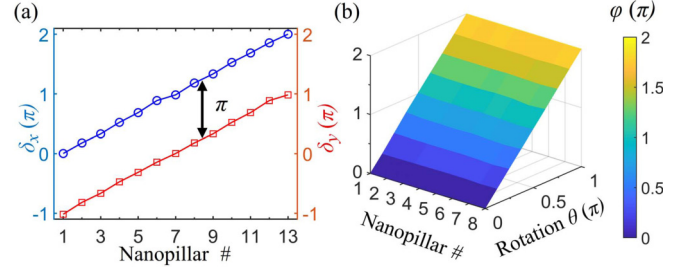


FIG. 5. (a) Numerically established phase delays δ_x and δ_y for selected nanopillars (1–13). A constant π -phase difference is observed between δ_x (circles, blue line) and δ_y (squares, red line). (b) Phase modulation φ for selected nanopillars as a function of the rotation angle θ .

that one might also consider using different heights or even different materials for the nanopillars to further optimize the performance of the proposed metasurface.

IV. RESULTS

We first consider basic HOP spheres on the order of $n = \pm 1$. For the HOP sphere with $n = +1$ as shown in Fig. 6(a), the points $(\pi/2, 0)$ and $(\pi/2, \pi)$ on the sphere are radial and azimuthal polarization states, which can be described by Eq. (4). For $n = -1$ as shown in Fig. 6(c), the polarization states at the same points on the sphere are the so-called π -radial and π -azimuthal polarizations [42]. The poles on both HOP spheres correspond to vortex beams of opposite circular polarization, whereas intermediate points between the poles and the equator represent different elliptically or linearly polarized vortex beams. Each point on the HOP spheres denotes a vortex beam of space variant polarization, represented by Eq. (6), with the state compactly described by Eq. (7) in the spherical coordinate system $(2\alpha, 2\Delta)$.

Two metasurfaces (named Meta1 and Meta2) were designed to generate different vector Bessel beams on the $n = \pm 1$ HOP spheres. To demonstrate that our method can, indeed, completely map out the entire HOP spheres and to characterize the fidelity of the metasurfaces, we select five incident beam polarization states [shown in Fig. 6(b)]. The polarization states are controlled by the QWP rotation angle β . The characterization of Meta1 for incident polarization states I–V are shown in Fig. 6(d). Numerically simulated intensity patterns and phase profiles are presented at different propagation distances z . It is readily observed that the polarization state changes with increasing z and the horizontal polarization forms a two-lobe pattern which rotates in the counterclockwise direction as expected from the theory. For instance, for case III when the distance z ranges from z_0 to $z_0 + 0.75z_p$, the intensity patterns and phase features comply with the vector mode evolution on the HOP sphere equator. Likewise, for the other incident polarization states, such as elliptical and circular polarization, all output beams match the vector modes described on the HOP sphere with $n = +1$.

The simulation results for Meta2, shown in Fig. 6, illustrate that our method can yield all beam modes on the $n = -1$ HOP sphere as well. Now, the output beams are superpositions of two opposite circular polarizations with topological

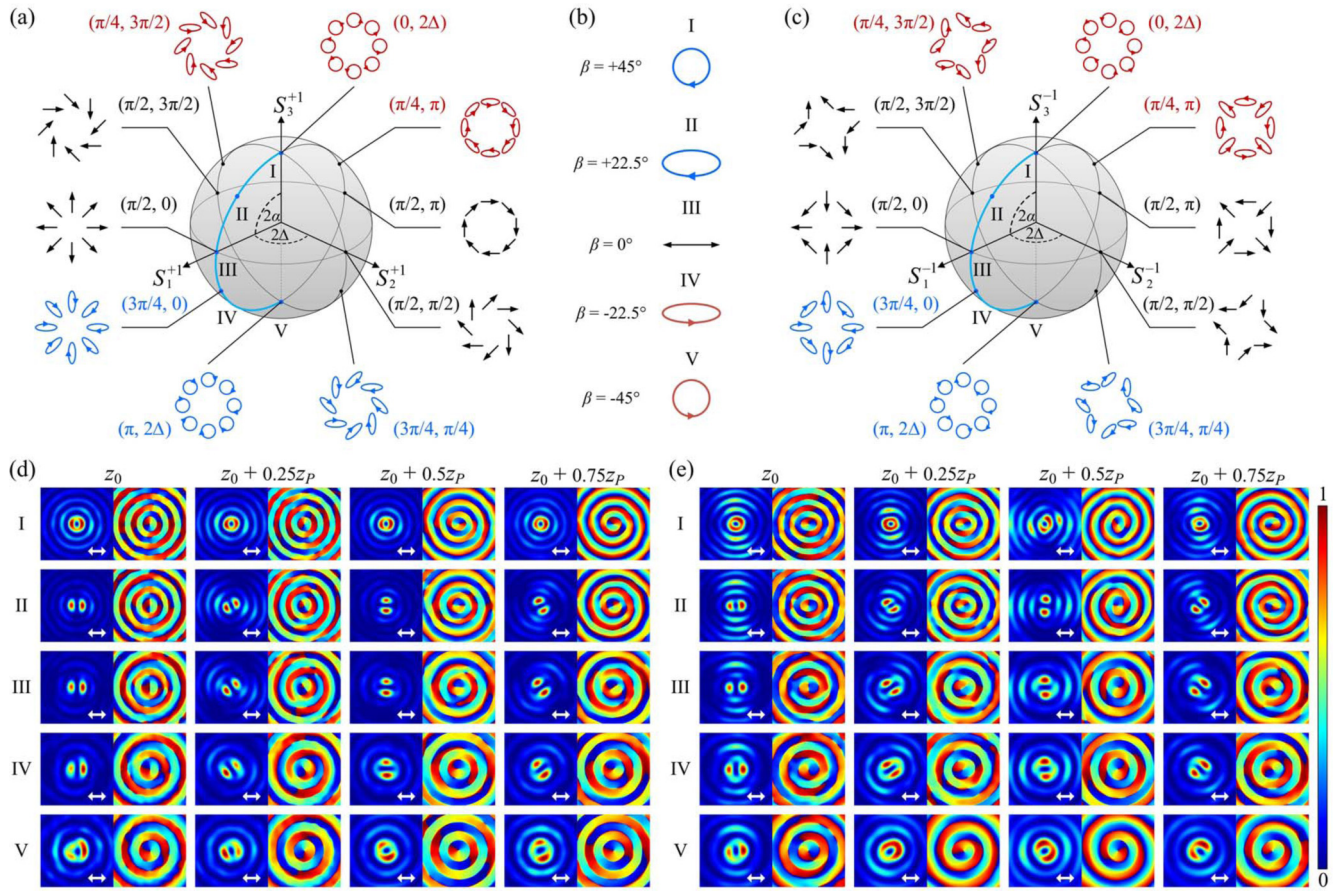


FIG. 6. (a) and (c) HOP sphere representations for the cases of $n = +1$ and $n = -1$. (b) Selected incident polarization states and the corresponding QWP rotation angles β . (d) and (e) Simulated output intensities (left) and phase profiles (right) after transmission through a horizontal linear polarizer; (d) for $n = +1$ and (e) for $n = -1$. Each row from left to right shows the results obtained for the ensuing vector Bessel beam as the propagation distance increases in steps from z_0 to $z_0 + z_P$. Rows I–V correspond to the selected incident polarization states as the QWP rotation angle is varied from $\beta = +45^\circ$ to -45° . The color bar indicates the normalized intensity (0 to 1) and the normalized phase ($0-2\pi$).

charge $n = \mp 1$. This can be explicitly confirmed from the phase profiles plotted for states I–V in Fig. 6(e). All annular intensity patterns are captured through a horizontal linear polarizer at different propagation distances z , indicating that the output beams show spatially variant polarization distributions which match the states on the $n = -1$ HOP sphere. Notably, at z_0 and $z_0 + 0.5z_P$, such output beams are π -radially and π -azimuthally polarized vector modes [42]. Comparing with the $n = +1$ case, the intensity pattern rotates clockwise with increasing z if a horizontally aligned linear polarizer is introduced.

Besides the basic $n = \pm 1$ HOP spheres, our metasurface design principle can further be utilized for the generation of any arbitrary higher-order HOP sphere beams. Cases I–III in Fig. 7(a) show the ensuing transverse intensity patterns at $z = z_0$ and $z = z_0 + 0.5z_P$ with RCP, horizontally polarized, and LCP beam illuminations, corresponding to $\beta = +45^\circ$, 0° , and -45° , respectively. We also calculate the OAM mode purity for the output beam modes at $z_0 + 0.5z_P$ by employing the modal decomposition method [43] (mode purity is defined as I_n/I_{total} , where I_n is the intensity of the mode n in question and I_{total} is the total beam intensity). As shown in Fig. 7(b), the mode purity for cases I and III reaches 99.8% and 99.9%

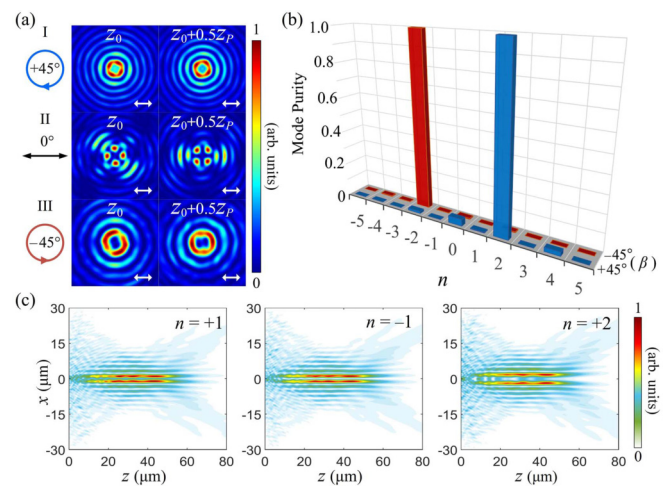


FIG. 7. (a) Transverse intensity patterns of output beams passing a horizontal linear polarizer, evaluated at two propagation distances z_0 and $z_0 + 0.5z_P$. Cases I–III correspond to $\beta = +45^\circ$, 0° , and -45° . (b) Mode purity analysis of the output beams at $z_0 + 0.5z_P$ for $\beta = \pm 45^\circ$. (c) Normalized intensity profiles of vector Bessel beams ($n = +1, -1, \text{ and } +2$) along the propagation direction.

for $n = \pm 2$. This means that we can achieve maximum mode purity for beams carrying OAM. Figure 7(c) shows the intensity profiles along the beam propagation direction for $n = +1$, -1 , and $+2$ HOP sphere beams, clearly displaying typical Bessel beam features. The results explicitly demonstrate that our metasurface designs can produce arbitrary HOP sphere vector Bessel beams whereas maintaining high beam quality.

V. CONCLUSIONS

We have put forward a general method to produce vector-Bessel beams that can cover all states on the HOP spheres of any given order n by a single all-dielectric metasurface. We have further demonstrated numerically the fidelity of the technique for silicon metasurfaces at telecom wavelength $\lambda = 1550$ nm. Although controlling the input polarization state (via adjusting a QWP rotation angle β) together with choosing the appropriate propagation distance z behind the planar metasurface, the output beams can assume any po-

larization states from the entire n th-order HOP sphere. This demonstrates a complete control over the vector nature and OAM of the output beams. Our method can be applied to any arbitrary order HOP spheres whereas maintaining high beam quality (mode purity in excess of 99.8% was simulated) and exhibiting the features characteristic of vector Bessel beams. It is also important to emphasize that lithographic fabrication of subwavelength dielectric nanowire patterns, including arrays of high aspect ratio elliptical nanopillars in silicon, is currently well established [44]. Based on these advantages, our approach may offer considerable potential for various applications in optical communication, laser processing and manipulation, and optical metrology.

ACKNOWLEDGMENTS

T.K.H. acknowledges the Academy of Finland (Project No. 322002). This work is part of the Academy of Finland Flagship Program “Photonics Research and Innovation” (PREIN, Project No. 320166).

-
- [1] J. Durnin, J. J. Miceli, Jr., and J. H. Eberly, Diffraction-Free Beams, *Phys. Rev. Lett.* **58**, 1499 (1987).
 - [2] J. Turunen and A. T. Friberg, Propagation-invariant optical fields, in *Progress in Optics*, edited by E. Wolf (Elsevier, Amsterdam, 2009), Vol. 54, pp. 1–88.
 - [3] M. Duocastella and C. B. Arnold, Bessel and annular beams for materials processing, *Laser Photonics Rev.* **6**, 607 (2012).
 - [4] D. McGloin and K. Dholakia, Bessel beams: Diffraction in a new light, *Contemp. Phys.* **46**, 15 (2005).
 - [5] Q. Zhan, Evanescent Bessel beam generation via surface plasmon resonance excitation by a radially polarized beam, *Opt. Lett.* **31**, 1726 (2006).
 - [6] W. Cheng, J. W. Haus, and Q. Zhan, Propagation of vector vortex beams through a turbulent atmosphere, *Opt. Express* **17**, 17829 (2009).
 - [7] Y. Zhao and J. Wang, High-base vector beam encoding/decoding for visible-light communications, *Opt. Lett.* **40**, 4843 (2015).
 - [8] Z. Bouchal, J. Wagner, and M. Chlup, Self-reconstruction of a distorted nondiffracting beam, *Opt. Commun.* **151**, 207 (1998).
 - [9] Q. Zhan, Cylindrical vector beams: From mathematical concepts to applications, *Adv. Opt. Photon.* **1**, 1 (2009).
 - [10] A. Holleczek, A. Aiello, C. Gabriel, C. Marquardt, and G. Leuchs, Classical and quantum properties of cylindrically polarized states of light, *Opt. Express* **19**, 9714 (2011).
 - [11] I. Moreno, J. A. Davis, M. M. Sánchez-López, K. Badham, and D. M. Cottrell, Nondiffracting Bessel beams with polarization state that varies with propagation distance, *Opt. Lett.* **40**, 5451 (2015).
 - [12] S. Tao, W. Lee, and X.-C. Yuan, Dynamic optical manipulation with a higher-order fractional Bessel beam generated from a spatial light modulator, *Opt. Lett.* **28**, 1867 (2003).
 - [13] R. Bowman, N. Muller, X. Zambrana-Puyalto, O. Jedrkiewicz, P. Di Trapani, and M. Padgett, Efficient generation of Bessel beam arrays by means of an SLM, *Eur. Phys. J.: Spec. Top.* **199**, 159 (2011).
 - [14] A. Dudley, Y. Li, T. Mhlanga, M. Escuti, and A. Forbes, Generating and measuring nondiffracting vector Bessel beams, *Opt. Lett.* **38**, 3429 (2013).
 - [15] S. Fu, S. Zhang, and C. Gao, Bessel beams with spatial oscillating polarization, *Sci. Rep.* **6**, 1 (2016).
 - [16] G. Milione, H. I. Sztul, D. A. Nolan, and R. R. Alfano, Higher-Order Poincaré Sphere, Stokes Parameters, and the Angular Momentum of Light, *Phys. Rev. Lett.* **107**, 053601 (2011).
 - [17] L. Allen, M. W. Beijersbergen, R. J. C. Spreeuw, and J. P. Woerdman, Orbital angular momentum of light and the transformation of Laguerre-Gaussian laser modes, *Phys. Rev. A* **45**, 8185 (1992).
 - [18] D. Naidoo, F. S. Roux, A. Dudley, I. Litvin, B. Piccirillo, L. Marrucci, and A. Forbes, Controlled generation of higher-order Poincaré sphere beams from a laser, *Nat. Photonics* **10**, 327 (2016).
 - [19] L. Feng, Y. Li, S. Wu, X. Guan, C. Yang, W. Tong, W. Li, J. Qiu, X. Hong, Y. Zuo, H. Guo, E. Chen, and J. Wu, All-fiber generation of arbitrary cylindrical vector beams on the first-order Poincaré sphere, *Photonics Res.* **8**, 1268 (2020).
 - [20] S. Lou, Yaqin Zhou, Y. Yuan, T. Lin, F. Fan, X. Wang, H. Huang, and S. Wen, Generation of arbitrary vector vortex beams on hybrid-order Poincaré sphere based on liquid crystal device, *Opt. Express* **27**, 8596 (2019).
 - [21] Z. Liu, Y. Liu, Y. Ke, Y. Liu, W. Shu, H. Luo, and S. Wen, Generation of arbitrary vector vortex beams on hybrid-order Poincaré sphere, *Photonics Res.* **5**, 15 (2017).
 - [22] R. Wang, S. He, S. Chen, J. Zhang, W. Shu, H. Luo, and S. Wen, Electrically driven generation of arbitrary vector vortex beams on the hybrid-order Poincaré sphere, *Opt. Lett.* **43**, 3570 (2018).
 - [23] R. Xu, P. Chen, J. Tang, W. Duan, S. Ge, L. Ma, R. Wu, W. Hu, and Y. Lu, Perfect Higher-Order Poincaré Sphere Beams from Digitalized Geometric Phases, *Phys. Rev. Appl.* **10**, 034061 (2018).

- [24] R. C. Devlin, A. Ambrosio, N. A. Rubin, J. B. Mueller, and F. Capasso, Arbitrary spin-to orbital angular momentum conversion of light, *Science* **358**, 896 (2017).
- [25] C. Pfeiffer and A. Grbic, Controlling Vector Bessel Beams with Metasurfaces, *Phys. Rev. Appl.* **2**, 044012 (2014).
- [26] S. Liu, A. Noor, L. L. Du, L. Zhang, Q. Xu, K. Luan, T. Q. Wang, Z. Tian, W. X. Tang, J. G. Han, W. L. Zhang, X. Y. Zhou, Q. Cheng, and T. J. Cui, Anomalous refraction and non-diffractive Bessel-beam generation of terahertz waves through transmission-type coding metasurfaces, *ACS Photonics* **3**, 1968 (2016).
- [27] Z. Ma, S. M. Hanham, P. Albella, B. Ng, H. T. Lu, Y. Gong, S. A. Maier, and M. Hong, Terahertz all-dielectric magnetic mirror metasurfaces, *ACS Photonics* **3**, 1010 (2016).
- [28] Y. Shen, J. Yang, H. Meng, W. Dou, and S. Hu, Generating millimeter-wave Bessel beam with orbital angular momentum using reflective-type metasurface inherently integrated with source, *Appl. Phys. Lett.* **112**, 141901 (2018).
- [29] X. Yang, Y. Zhou, and G. Wang, A wideband transmission metasurface for generating Bessel beam carrying orbital angular momentum, *Int. J. RF Microw. C. E.* **29**, e21941 (2019).
- [30] Z. Lin, X. Li, R. Zhao, X. Song, Y. Wang, and L. Huang, High-efficiency Bessel beam array generation by Huygens metasurfaces, *Nanophotonics* **8**, 1079 (2019).
- [31] W. T. Chen, M. Khorasaninejad, A. Y. Zhu, J. Oh, R. C. Devlin, A. Zaidi, and F. Capasso, Generation of wavelength-independent subwavelength Bessel beams using metasurfaces, *Light Sci. Appl.* **6**, e16259 (2017).
- [32] C. Spägle, M. Tamagnone, D. Kazakov, M. Ossiander, M. Piccardo, and F. Capasso, Multifunctional wide-angle optics and lasing based on supercell metasurfaces, *Nat. Commun.* **12**, 3787 (2021).
- [33] A. Arbabi, Y. Horie, M. Bagheri, and A. Faraon, Dielectric metasurfaces for complete control of phase and polarization with subwavelength spatial resolution and high transmission, *Nat. Nanotechnol.* **10**, 937 (2015).
- [34] J. H. McLeod, The axicon: A new type of optical element, *J. Opt. Soc. Am.* **44**, 592 (1954).
- [35] Z. Jaroszewicz, *Axicons: Design and Propagation Properties* (SPIE, Warsaw, 1997).
- [36] Z. Jaroszewicz, A. Burvall, and A. T. Friberg, Axicon—the most important optical element, *Opt. Photonics News* **16**, 34 (2005).
- [37] A. Vasara, J. Turunen, and A. T. Friberg, Realization of general nondiffracting beams with computer-generated holograms, *J. Opt. Soc. Am. A* **6**, 1748 (1989).
- [38] *Handbook of Optical Constants of Solids*, edited by E. D. Palik, (Academic, Orlando, 1998).
- [39] A. I. Kuznetsov, A. E. Miroshnichenko, M. L. Brongersma, Y. S. Kivshar and B. Luk'yanchuk, Optically resonant dielectric nanostructures, *Science* **354**, aag2472 (2016).
- [40] M. Decker, I. Staude, M. Falkner, J. Dominguez, D. N. Neshev, I. Brener, T. Pertsch, and Y. S. Kivshar, High-efficiency dielectric Huygens surfaces, *Adv. Opt. Mater.* **3**, 813 (2015).
- [41] G. Biener, A. Niv, V. Kleiner, and E. Hasman, Formation of helical beams by use of Pancharatnam-Berry phase optical elements, *Opt. Lett.* **27**, 1875 (2002).
- [42] B. J. Roxworthy and K. C. Toussaint, Jr., Optical trapping with π -phase cylindrical vector beams, *New J. Phys.* **12**, 073012 (2010).
- [43] Y. Liu, C. Gao, M. Gao, and F. Li, Coherent-mode representation and orbital angular momentum spectrum of partially coherent beam, *Opt. Commun.* **281**, 1968 (2008).
- [44] E. Schonbrun, K. Seo, and K. B. Crozier, Reconfigurable imaging systems using elliptical nanowires, *Nano Lett.* **11**, 4299 (2011).